Cognitive flexibility through metastable neural dynamics is disrupted by damage to the structural connectome

Abbreviated title: The connectome, metastability and cognitive flexibility

Author names and affiliations: Peter J. Hellyer [1,2] *, Gregory Scott [1] *, Murray Shanahan [3], David J. Sharp [1], Robert Leech [1]

* These authors contributed equally to the work presented in this report.

1. Computational, Cognitive, and Clinical Neuroimaging Laboratory, Division of Brain Sciences, Faculty of Medicine, Imperial College London, Hammersmith Hospital Campus, Du Cane Road, London, W12 0NN, UK
2. Centre for Neuroimaging Sciences, Institute of Psychiatry, Psychology and Neuroscience, King's College London.
3. Department of Computing, Imperial College London, 180 Queen's Gate, London, SW7 2RH, UK

Corresponding author: Robert Leech, Computational, Cognitive and Clinical Neuroimaging Laboratory, 3rd Floor, Burlington Danes, Hammersmith Hospital, Du Cane Road, London W12 0NN, UK. E-mail: r.leech@imperial.ac.uk. Tel: +44 (0)207 594 7994

Number of pages: 47

Number of figures: 9,

Number of words: Abstract: 152 **Introduction:** 650 **Discussion:** 1,500

Conflict of Interest: The authors declare no competing financial interests.

Acknowledgements: PJH was supported by a Medical Research Council Doctoral Training Award. GS was supported by a clinical research fellowship awarded in the Wellcome Trust-GlaxoSmithKline Translational Medicine Training Programme. We would like to thank Frantisek Vasa for useful conversations on comparing simulated and empirical networks, as well as thanking the participants who were involved in this research.

Abstract

Current theory proposes that healthy neural dynamics operate in a metastable regime, where brain regions interact to simultaneously maximise integration and segregation. Metastability may confer important behavioural properties, such as cognitive flexibility. It is increasingly recognised that neural dynamics are constrained by the underlying structural connections between brain regions. An important challenge is, therefore, to relate structural connectivity, neural dynamics and behaviour. Traumatic brain injury (TBI) is a pre-eminent structural disconnection disorder, whereby traumatic axonal injury damages large-scale connectivity, producing characteristic cognitive impairments, including slowed information processing speed and reduced cognitive flexibility, that may be a result of disrupted metastable dynamics. Therefore, TBI provides an experimental and theoretical model to examine how metastable dynamics relate to structural connectivity and cognition. Here, we use complimentary empirical and computational approaches to investigate how metastability arises from the healthy structural connectome and relates to cognitive performance. We found reduced metastability in large-scale neural dynamics after TBI, measured with resting-state functional MRI. This reduction in metastability was associated with damage to the connectome, measured using diffusion MRI. Furthermore, decreased metastability was associated with reduced cognitive flexibility and information processing. A computational model, defined by empirically-derived connectivity data, demonstrates how behaviourally-relevant changes in neural dynamics result from structural disconnection. Our findings suggest how metastable dynamics are important for normal brain function and contingent on the structure of the human connectome.

Introduction

To understand how cognitive-emotional functions emerge from the brain and are affected by disease requires an account of how neural ensembles act in concert to generate behaviour (Uhlhaas and Singer, 2006; Deco et al., 2008; Chialvo, 2010; Tognoli and Kelso, 2014). One approach is to consider the brain as a complex system (Friston, 1997; Chialvo, 2010). In this framework, current theory suggests an essential property of neural activity is *metastability,* a dynamical regime in which neural ensembles are able to coordinate rapidly, flexibly engaging and disengaging without becoming locked into fixed interactions (Friston, 1997; Shanahan, 2010; Tognoli and Kelso, 2014). Metastability is thought to confer optimal information processing capabilities, flexible behaviour and memory (Werner, 2007; Deco et al., 2009a; Shanahan, 2010). However, there is little empirical evidence to support this hypothesis. We have previously shown, with both empirical and computational approaches that metastability at rest is higher than during a focused cognitive task (Hellyer et al., 2014). During a task, high metastability may be undesirable, where instead a specific configuration of brain systems is maintained over time (e.g., in coordinating specific visual and motor systems to perform a visually cued motor task).

Theoretical studies demonstrate that the emergence of metastable dynamics is contingent on the coupling between modules of a dynamical system (Friston, 1997; Strogatz, 2001; Shanahan, 2010; Cabral et al., 2011). In particular, dynamic patterns of functional connectivity, consistent with metastable dynamics, emerge when coupling has “small-world” topology with short average path lengths and high clustering (Wildie and Shanahan, 2012) of modules. Recently, networks of anatomical connections have been incorporated within computational simulations of large-scale neural dynamics, suggesting metastable dynamics provide a link between

structural and functional connectivity (Deco et al., 2009b; Honey et al., 2009; Cabral et al., 2011; Hellyer et al., 2014).

The disruption of neural dynamics is thought to be important in brain disorders (Uhlhaas and Singer, 2006), likely caused by abnormal structural connectivity (Friston, 2002; Bassett and Bullmore, 2006; Cabral et al., 2012; Sharp et al., 2014). Indeed, through the examination of brain disorders, we are able to explore the importance of structural connectivity for the organisation of functional connectivity. A large body of work has examined the link between focal damage to the brain, such as in ischemic stroke, and cognition (Bird et al., 2004; Sharp et al., 2010a; Gratton et al., 2012; Warren et al., 2014). However, structural disconnection is often intermingled with gray matter damage (Sharp et al., 2011; Bonnelle et al., 2012). In contrast, traumatic brain injury (TBI) frequently results in diffuse axonal injury (DAI), which disrupts long-distance white matter tracts connecting brain regions (Sharp et al., 2011; Johnson et al., 2013b; Johnson et al., 2013a) but with neuronal bodies relatively spared. As such, it is a preeminent example of a white matter disconnection disorder (Sharp et al., 2014). Damage to white matter connectivity in TBI alters the spatiotemporal properties of functional brain networks (Kinnunen et al., 2011; Hellyer et al., 2013; Caeyenberghs et al., 2014; Jilka et al., 2014), resulting in long-term cognitive problems, including impairments in cognitive flexibility, memory and information processing speed (Bonnelle et al., 2011; Kinnunen et al., 2011; Jilka et al., 2014). Cognitive inflexibility after TBI may be observed as poor performance on tests of task switching (Kinnunen et al., 2011; Hellyer et al., 2013; Caeyenberghs et al., 2014; Jilka et al., 2014). Extreme inflexibility may manifest as *perseveration*, the repetition of a particular response, such as a phrase or gesture, despite the cessation of a stimulus. Therefore, TBI provides an ideal paradigm to examine how three

important levels of description – structure, functional dynamics and behaviour – converge.

Here, using empirical and computational approaches, we investigate how metastability, defined as the standard deviation of the Kuramoto order parameter (as in (Shanahan, 2010; Cabral et al., 2011)), arises from the structural connectome and relates to behaviour. We test whether: (i) structural disconnection following TBI (measured using diffusion tensor imaging) is associated with reduced metastability (measured using resting-state fMRI); (ii) metastability is associated with behavioural measures of cognitive flexibility, memory and information processing. Furthermore, we use computational simulations to investigate the consequences of structural disconnection on large-scale neural dynamics, to demonstrate how disconnection following TBI results in altered metastability.

Materials and Methods

Overview

Our experimental approach is split into three different sections, described in detail below. An overview of the Methods is provided in Figures 1 and 2. In brief, firstly, we use resting state functional MRI (fMRI) to estimate empirical measures of metastability in healthy control subjects and in the presence of structural disconnection in TBI patients (Figure 1A&C). Secondly, we use a diffusion tensor imaging (DTI) approach to estimate both voxelwise (FA) and region of interest (ROI) level connectivity for each subject (Figure 2). Finally, we employ a range of both computational (using the Kuramoto model of phase oscillators) and empirical imaging based approaches, to describe the relationship between structural connectivity, metastability and neuropsychological performance (Figure 1C)

Image acquisition

Standard protocols were used to acquire functional, structural and diffusion tensor MRI data using a Phillips Intera 3.0 Tesla MRI scanner, with an 8-array head coil, and sensitivity encoding (SENSE) with an under sampling factor of 2. For each participant, diffusion-weighted volumes with gradients applied in 64 non-collinear directions were collected. The following parameters were used: 73 contiguous slices, slice thickness=2mm, field of view 224mm, matrix 128×128 (voxel size=1.75×1.75×2mm^3), b value=1000 and four images with no diffusion weighting (b=0s/mm2). Earplugs and padded headphones were used to protect participants' hearing during the scanning procedure. We additionally collected a standard high-resolution T1 image for segmentation and image co-registration. During the resting state fMRI scan, subjects were asked to keep their eyes closed and to try not to fall asleep. Functional volumes were collected using a T2*-weighted gradient-echo-

planar imaging sequence with whole-brain coverage (repetition time/echo time, 2,000/30 ms; 31 ascending slices with thickness 3.25 mm, gap 0.75 mm, voxel size 2.5×2.5×5mm, flip angle 90°, field of view 280×220×123 mm, matrix 112×87). Quadratic shim gradients were used to correct for magnetic field inhomogeneities within the brain.

Participants

63 traumatic brain injury (TBI) patients (16 female, mean age ±SD: 37.4±12.37 years) and 26 healthy control subjects (12 female, mean age ±SD: 35.96±17.61 years) were scanned using standard functional and structural MRI protocols (see below). The patients and controls overlapped with those used in Fagerholm et al (in press, Brain), where group demographics are reported in more detail. At the group level, patients and controls were matched for age (t_{87}=-0.47, p=0.64) and gender. We did not hypothesise that there would be any effects of handedness, and so did not select subjects according to handedness. TBI patients were scanned in the chronic phase, 5.48±3.33 (months ±SD) post injury. Injury severity of TBI patients was classified according to the Mayo system (Malec et al., 2007): “Moderate-severe” (55 patients); “Mild (probable)” (5); and “Symptomatic (possible)” (3). 49 patients had a clinically relevant episode of post-traumatic amnesia (PTA) following TBI. Where the mechanism of injury was known, the mechanism was: road traffic accident (21 patients); assault (17); fall/syncope (15); sports injury/concussion (2); unknown (8). All participants gave written consent, were checked for contraindications to MRI scanning and had no history of significant neurological or psychiatric illness prior to TBI. The Hammersmith, Queen Charlotte’s and Chelsea research ethics committee awarded ethical approval for the study.

Neuropsychological assessment

All but one patient (62, mean age ±SD: 37.53±12.45 years) performed a paper and pencil, neuropsychological test battery. Our analysis focused on cognitive measures shown previously to be sensitive to impairments following TBI: Associative memory (AM), using the immediate recall and retention measure of the People Test from the Doors and People Test (Baddeley, 1986, 1992; Baddeley et al., 1994) and Executive function (EF), using the Trail Making Test alternating switch-cost index (Reitan, 1958). In addition, a subset of 49 patients also completed the computerised Choice Reaction Time (CRT) task that assesses speed of processing (Rabbitt, 1966; Logan et al., 1984). It was for technical reasons, for example, relating to equipment error, that not all subjects completed all three neuropsychological tests. Neuropsychological assessment was performed immediately prior to the MRI scanning session by a trained experimenter; scoring for each test was performed according to the protocols provided by the original publisher of each test and no further selection based on neuropsychological outcome was performed. We present all collected data for each of these groups (i.e., no statistical subsampling on the basis of performance on any individual test has been performed).

Analysis of functional imaging data (Figure 1A)

Pre-processing of functional data was performed according to standard analysis approaches: briefly, this included realignment of EPI images to remove the coarse effects of motion between scans using FMRIB's Motion correction tool MCFLIRT (Smith et al., 2004). T1 images for each subject were segmented into 164 cortical and subcortical regions using the Destreux Freesurfer atlas (Fischl et al., 2004). The segmented T1 images were registered to the motion corrected data using boundary-based registration (Greve and Fischl, 2009). Subsequently, mean BOLD time series for each region of interest (ROI) were extracted from the resting state scans. We

band-pass filtered the data between 0.01 and 0.2 Hz to remove sources of non-neural noise and focus on slow modulations in BOLD, that have previously been associated with intrinsic connectivity networks (Niazy et al., 2011). Such band-pass filtering is an important step in transforming raw time series into phase space (see below). To account for variance related to head motion or non-neural physiological noise, during pre-processing we regressed out from the time course for each of the 164 ROIs, the six motion parameter time courses estimated by MCFLIRT (Smith et al., 2004), the motion parameters squared as well as time series sampled from regions of white-matter and cerebrospinal fluid. To further reduce the possibility that effects are driven by head motion we controlled for motion at the group level, (i.e. across subjects) by including the estimate of mean framewise displacement in higher-level analyses as a regressor of no interest.

To facilitate comparison of measures of metastability and synchrony between the computational model and empirical data, we transformed the empirical data into a complex phase representation, so the same analysis can be applied to both the empirical and computational simulation data. The transformation of functional neuroimaging data into phase representation for analysis has been previously performed using a variety of different approaches such as wavelet analysis (Kitzbichler et al., 2009; Chang and Glover, 2010), as well as the computationally simpler Hilbert transform on bandpass filtered data (Glerean et al., 2012). For simplicity, we perform the latter on each of the bandpass filtered 164 ROI time series from the empirical data, resulting in 164 phase time series. Measures of network dynamics were either calculated on all regions simultaneously (global) or within specific predefined intrinsic connectivity networks (local).

Definition of intrinsic connectivity networks from functional imaging data

We defined a set of intrinsic connectivity networks (ICNs) from the resting state fMRI data, to allow us to optimise the computational model and to define networks from which to sample neural dynamics. To do this, we performed temporal concatenation independent component analysis (ICA) on each of the 164 ROI mean BOLD time-series for an independent group of 10 healthy control subjects, using FSL MELODIC (Beckmann et al., 2005). The optimal decomposition estimated during Fast ICA resulted in the identification of 15 independent networks. These ICNs were used to tune the computational model (see below). Resulting components were thresholded at $z>2.3$, and surviving brain regions were included in that network. Each of these networks were then labelled by eye based on their resemblance to the canonical ICNs produced by (Smith et al., 2009). This resulted in the identification of seven canonical ICNs which were used in subsequent analyses (Visual, Auditory, Default Mode, Dorsal Attention, Salience and both Left and Right fronto-parietal control networks - Figure 3). These networks were used to sample metastability for both the empirical and simulated data.

Estimation of healthy structural connectivity network (Figure 2A)

The mean location and probability of structural connections was estimated in a further group of 10 independent healthy control subjects (Figure 2A). Structural T1 images were segmented into white matter and the same 164 cortical and subcortical gray matter ROIs as used to sample the fMRI data, using Freesurfer (Greve & Fischl, 2009). This produced a mask for each region in each participant's T1 native space. Diffusion imaging data was reconstructed using the FSL diffusion toolkit using standard protocols (Behrens et al., 2003b). We further modelled the probability distribution of fibre direction within each voxel in order to account for crossing fibres (Behrens et al., 2003a). Non-linear registration was used to calculate a warp-field

between conformed Freesurfer space and the DTI b0 image, using the FSL non-linear Image registration tool (Smith et al., 2004). The warp-field was then applied to masks for white matter and each of the 164 cortical and subcortical ROIs using nearest-neighbour interpolation. Individual gray matter masks were dilated by a single voxel and multiplied by the white matter mask, in order to generate ROIs to be used as seeds and targets for tractography at the boundary between white and gray matter surfaces (Gong et al., 2009).

Probabilistic tractography, using 5000 random streamline samples per voxel was used to estimate the connectivity matrix$\langle C \rangle$ between each of the 164 other regions alongside a spatial distribution of connective fibres between each region. The probability of connections between two regions $C_{(i,j)}$ was defined as the proportion of all fibres sent from region i which successfully reached region j. As probabilistic tractography cannot determine directionality of connections between cortical regions and the size of seed and target ROIs may differ for each connection, we define $C_{(i,j)}$ as the mean of the forward and reverse connections between regions, i.e. .$C_{(i,j)} = \frac{1}{2}(C_{(i,j)} + C_{(j,i)})$. To minimise the number of false positive connections, a thresholding approach was used to generate a binary matrix that retained connections with a consistent probability across all subjects from the tractography group (Gong et al., 2009). This resulted in a connectivity matrix with a density of 26%. This is comparable with previously published datasets such as (Hagmann et al., 2008) – 26% and (van den Heuvel and Sporns, 2011) 14-21%. The relationship between the number of streamlines and the underlying information propagating properties of the tracts is unclear and this is likely to be a particular problem for long-distance connections (Gigandet et al., 2008; Jones, 2010b, a). For this reason, we binarized our reference connectivity dataset. The length matrix (i.e., the length of tracts between pairs of regions) was estimated using the Euclidean distance between

the centres of gravity of each individual ROI in standard MNI152 space. Euclidean distance is inexact, since tracts are not likely to follow the shortest distance between regions, but it is a good first approximation of the distances and has been used extensively in a range of similar computational modelling approaches (Deco et al., 2008; Deco et al., 2009b; Cabral et al., 2011).

Estimation of individual structural connectivity (Figure 2B)

Global and focal reductions of fractional anisotropy (FA) in TBI patients have been shown to bias tractography estimation in TBI patients (Squarcina et al., 2012), potentially resulting in spurious differences including false increases in structural connections following injury. This previous work suggested that sampling FA along a known tract distribution estimated from an independent group of healthy control subjects is preferable to estimating tracts from TBI patients themselves. Therefore, we sampled FA projected through a set of tracts linking the 164 regions, defined on the independent group of 10 healthy controls. First, we used Tract-Based Spatial Statistics (TBSS) (Smith et al., 2006) to align the FA map of each patient and control subject to a common template. In order to reduce partial volume effects, these tracts were then skeletonized, resulting in a voxel-wise map of the white matter skeleton for each subject (Figure 4).

We used random permutation testing (Nichols and Holmes, 2002; Smith et al., 2004; Winkler et al., 2014) to assess whether there was reduced FA in patients compared to controls (Kinnunen et al., 2011; Hellyer et al., 2013). We fitted a general linear model for each voxel within the skeleton. Whilst this approach gives a good overview of spatial distribution of damage, we further wished to estimate integrity of individual pre-defined ‘tracts’ for each patient and control, to define a structural connectivity matrix. Therefore, mean FA values were calculated from masks generated at the

intersection of voxels of the skeletonised map and each tract region of interest (as defined using tractography on independent controls, see the previous section). This resulted in a 'tract integrity' FA matrix for each patient and control (Figure 2C). In order to define 'damage' to tracts, rather than use an arbitrary threshold of these matrices (which is likely to remove valid tracts in both the patient and control population with naturally low FA, due to factors such as crossing fibres), we determined the tracts within which damage is likely, by estimating the normal distribution (mean and standard deviation) of FA values for each connection within the independent group of healthy controls (used to define the tractography). This information was then used to z-transform the FA values for each tract within each individual subject in the patient and control group. To simulate damage to the connectivity matrix $\langle C \rangle$, if any edge from the scaled FA matrix for an individual fell below a certain threshold (-1.6SD, which represents the position within the normal Gaussian distribution, where an individual event is distinct from noise with a nominal probability of approximately $p<0.05$) it was 'lesioned'. Rather than removing the tract (which is overly destructive given the nature of the traumatic axonal injury, where the tract typically remains but shows evidence of damage) we instead reduced connectivity by a fixed amount (Figure 2C). This has the effect that each connectivity matrix has the same number of connections, while capturing any pattern of damage. Results reported are for a reduction of 50%, but the results were robust to a range of different damage values.

Graph theoretic metrics for structural connectivity

In order to define changes in structural connectivity in relation to changes in neural dynamics, we assessed large scale structural connectivity using measures from graph theory, calculated using the Brain Connectivity Toolbox (Rubinov and Sporns, 2010). These measures are described briefly below:

Degree (D).

$$D_i = \sum_{j=1}^{N} C_{i,j}$$

The degree of each node D_i within a weighted graph $\langle \mathrm{C} \rangle$, is defined as the sum of all directly connected edges to the node within the network. The mean degree defines how strongly interconnected all nodes within the network are (Freeman, 1978).

Characteristic path length ($\bar{L}$)

$$L_i = \frac{\sum_{v \neq w} D(v,w)}{|V(C)| - 1}$$

Path length (L_i) is the average distance of an individual vertex to all its connected neighbours ($v \in V(C)$) in a network $\langle \mathrm{C} \rangle$, weighted by the inverse of the weight of connectivity (D) i.e. higher weight connections are interpreted as a shorter connection length. The mean of this value across all nodes ($\bar{L}$) is the measure of characteristic path length within a network (Watts and Strogatz, 1998).

Clustering coefficient ($\bar{K}$)

$$K_i = \frac{2e_i}{k_i(k_i - 1)}$$

The weighted clustering coefficient of a node (K_i) is the average connectivity strength of all "triangles", i.e. all neighbours (e_i) which also directly connect to each other as

pairs (k_i) around a specific node (i). The mean across nodes ($\overline{K}$) is used as a measure of network clustering (Watts and Strogatz, 1998).

Small-worldness ($\boldsymbol{\sigma}$)

$$\sigma = \frac{K.\hat{K}^{-1}}{L.\hat{L}^{-1}}$$

Small-world networks have low characteristic path length and high clustering coefficient. An often applied metric of 'small-worldness' is the small world index (σ - SWI), (Sporns, 2006; Humphries and Gurney, 2008). This compares the path length (L) and clustering coefficient (K) to equivalent measures of a suitable Erdös-Rényi random network (Humphries and Gurney, 2008) ($\hat{K}$ and $\hat{L}$ repectively). If $\sigma > 1$, a network is considered small-world.

Differences in σ, and $\overline{K}$ may be artifactually driven by reduction in the mean degree of individual networks. In order to correct for this potential source of estimation error, we controlled for variation of mean degree across each subject's structural connectivity graph by normalising the mean degree of each graph (i.e. dividing $\langle C \rangle$ by the mean of connected vertices in D) before calculating σ, and $\overline{K}$. In this way, changes in each of these measures will be driven by altered network topology, rather than simply global changes in connectivity strength.

Computational simulation of neural dynamics (Figure 1B)

In order to explore the effect of structural disconnection on neural dynamics, we used the simple Kuramoto model of coupled phase oscillators (Acebrón et al., 2005). We chose this model, partly as it has been shown to be able to simulate macroscopic neural dynamics related to underlying structural connectivity (Shanahan, 2010; Cabral et al., 2011; Hellyer et al., 2014; Messe et al., 2014). It has also been shown to capture the same essential aspects of macroscopic dynamics as far more complex

models based on tens of thousands of simulated neurons (Bhowmik and Shanahan, 2013). Compared to such complex and computationally far more intensive models, the Kuramoto model provides a good trade off between complexity and plausibility, modelling a few key parameters of structural and functional relationships between nodes. By using the less computationally intensive Kuramoto model we were able to explore large parameter spaces and simulate many individual subjects' dynamics. The activity of each of the 164 brain regions (which we define here as a node) is represented in our model by the phase of a Kuramoto oscillator. The phase of each node over time is described by the Kuramoto equation (Kuramoto, 1984; Acebrón et al., 2005):

$$\frac{d\theta_i}{dt} = \omega_i + \frac{1}{N+1}\sum_{j=1}^{N}\left(C_{i,j}\right)\sin\left(\theta_{(j)}(t - D_{i,j}) - \theta_i(t)\right) \quad N = 164$$

The natural frequency ω defines the phase change of an un-coupled node per time-step. In our simulations, as in previous work (Cabral et al., 2011), we fixed the natural frequency to match known oscillations within the gamma frequency range (ω = 60Hz). The connectivity matrix $\langle C \rangle$ is a binary connectivity matrix determined by the empirical strength of white matter connections, or lesioned using individual tract integrity data (see above). The distance matrix $\langle D \rangle$, determined by the empirical length of connections between regions, imposes time delay on phase interactions between nodes. This is analogous to the simulation of a delay caused by neural conduction between regions of the brain.

We introduce two control parameters to the coupling and delay of the network; the global coupling parameter (k), and mean global velocity $\langle v \rangle$, such that $\langle C \rangle = k\langle C \rangle$ and $\langle D \rangle = \langle D \rangle / v$. The behavior of the Kuramoto model in terms of global metastability and synchrony, by modulation of the parameters k and v, has been explored previously (Shanahan, 2010; Cabral et al., 2011). For completeness, we also present a traversal

of this parameter space (Figure 8), using the baseline binary connectivity dataset defined using 10 healthy controls (see: 'Estimation of healthy structural connectivity network' above). The presence of multiple local maxima of both metastability and synchrony within the $\langle k, v \rangle$ plane makes it challenging to optimise though a gradient-descent approach. Therefore, we randomly selected 6000 pairs of model parameters within the $\langle k, v \rangle$ plane and executed the model for each pair. We then used nearest neighbour interpolation to create the parameter space $\langle k, v \rangle$ presented in Figure 8.

Validation of computational simulation

To validate the computational simulation against empirical functional connectivity derived from fMRI BOLD data, we followed the approach to simulating BOLD activity previously demonstrated in the literature (e.g.,(Cabral et al., 2011)), using the sine of the high-frequency activity of the Kuramoto model as the neural input to the Balloon-Windkessel haemodynamic model (Friston et al., 2000), low-pass filtered the resulting time courses at <0.25 Hz, and downsampling to a 2 second sampling rate.

Unlike previous approaches to model validation that have assumed that the spatio-temporal organisation of correlations within empirical fMRI BOLD time courses are univariate, we used an ICA approach to compare empirical BOLD activity (defined using the ICA decomposition described above) with the output of our computational models. Simulated BOLD time-courses from each of the computational models were decomposed into 15 spatially independent time-courses. Spatial components from the empirical and modelled ICAs were then 'matched' using spatial correlation of their maps. Since the order of components extracted by MELODIC varies, we determined maximal correspondence between empirical and model components by calculating the pair-wise spatial correlation between functional connectivity maps for all pairs of components and reordering the resulting correlation matrix so as to maximize entries along the diagonal. An evaluation function was defined as the mean correlation

between the empirical spatial maps and the modeled spatial maps for the top *n* (here n=5) matched components in the computational model compared to the empirical data, providing an objective measure by which the fit of individual regions of the global parameter space to empirical data may be compared against one another (Figure 8). We present the results for ICA using 15 components in both empirical and modelled data, and n = 5; however, varying each of these parameters produced qualitatively similar results.

Synchrony and metastability measures of neural dynamics (Figure 1C)

The order parameters $R(t)$ and $\Phi(t)$ can be jointly defined by:

$$R(t)e^{i\Phi(t)} = \frac{1}{N}\sum_{n=1}^{N} e^{i\Theta_n(t)}$$

Where N is the total number of regions within the network and the level of synchrony between phase time courses is described by $R(t)$, in terms of how coherently phase changes over time (Shanahan, 2010; Cabral et al., 2011). During fully synchronous behaviour $R(t) = 1$; whereas $R(t) = 0$ where phase across all phase time series is fully asynchronous. The phase of all the input phase time series is described by $\Phi(t)$ but is not used in the present work. For both empirical and simulated timeseries, we measured neural dynamics in terms of mean global synchrony ($\overline{R}$), and global metastability as the standard deviation σ_R of global synchrony across the same period (Shanahan, 2010; Cabral et al., 2011). In addition to global measures of dynamics, to evaluate measures of network dynamics in both the empirical and simulated data, we calculated separate mean synchrony and metastability measures for the phase timeseries of regions within the 7 empirical ICNs defined earlier (See 'Definition of intrinsic connectivity networks from functional imaging data')

Results

Widespread disruption to the structural connectome after traumatic brain injury

To demonstrate that white matter connectivity is disrupted following traumatic brain injury (TBI) in the group of patients studied, we performed standard tract-based spatial statistics (TBSS) to compare white matter integrity, measured by fractional anisotropy (FA), between patients and healthy controls, using age and total gray matter volume as covariates of no interest. In the between-group contrast of Patients < Controls, there was widespread reduction in FA across the white matter skeleton (Figure 4A). FA reduction was particularly pronounced in the inter-hemispheric fibres of the corpus callosum (where damage was widespread, but most extensive in the body and genu), as well as tracts within the superior longitudinal fasiculus, corticospinal tract, and the anterior and posterior limbs of the internal capsule. Additionally, a strong reduction of FA was observed within the fornix and corona radiata. This distribution of widespread changes to white matter integrity is typical of injury following TBI and is consistent with our previous TBSS-based findings (Kinnunen et al., 2011).

To explore how network level measures of structural connectivity are changed following TBI, we tested for group-wise differences between graph theoretical measures of large-scale structural connectivity between healthy controls and TBI patients using age as a covariate of no interest. There was a significant reduction in patients compared to controls in small-worldness (t_{86}=-3.10, $p<0.01$), clustering coefficient (t_{86}=-2.04, $p<0.05$) and mean degree (t_{86}=-3.42, $p<0.001$). In addition, patients had a significantly higher characteristic path length compared to healthy controls (t_{86}=3.07, $p<0.01$).

Empirical measures of metastability of large-scale neural dynamics are reduced following traumatic brain injury

We assessed the metastability of large-scale neural dynamics following TBI, measured using 164 regional phase time courses derived from resting-state fMRI BOLD data in both patients and controls (Figure 1A). We compared metastability across the whole brain and within ICNs between patients and controls, including age, gray matter volume and mean absolute movement as covariates of no interest. Global metastability was significantly reduced in TBI patients compared to controls (t_{84}=-2.63, $p<0.05$ 1-tailed), Figure 5. Patients also showed lower metastability in the salience network (t_{84} = -3.68 $p<0.001$), a left fronto-parietal network (t_{84} = -2.41, $p<0.02$) and dorsal attention network (t_{84} = -2.27, $p<0.05$); these survive multiple comparison correction by FDR ($q<0.1$). A potential confound for measuring widespread neural dynamics in the TBI patient population is the presence of cortical contusions. Thirty-two patients in the TBI group were found to have focal gray matter lesions, suggestive of cortical contusions, on T1-weighted structural imaging. It is possible that these lesions affected the BOLD time courses extracted and the resulting metastability calculations. We therefore repeated the calculation of global metastability after removing brain regions whose anatomical segmentation overlapped with focal lesions in any patients (Figure 4B) (i.e., time courses from affected regions were not analysed in any patients or controls). Reduction in global metastability in TBI patients compared to controls following this adjustment was similar to the original analysis (t_{84}=-2.63 $p<0.01$).

To establish whether the differences we report were due to changes in metastability (i.e., temporal variability in how synchronous the brain is) rather than simple temporal variability in the BOLD signal, we performed a follow up analysis. We calculated the standard deviation of: a) the mean BOLD signal across all 164 regions; and b) the

mean BOLD signal of each region. In a GLM using age, gray matter volume and mean absolute displacement as covariates of no interest, we found no group-wise effect in the standard deviation of the mean global BOLD signal (t_{84}=0.22 p=0.82). For each of the 164 regions, no single region showed a significant effect of group (FDR correcting for multiple comparisons; even without correcting for multiple comparisons only four regions had a group-wise effect with p lower than 0.05 with the lowest value p=0.04).

Empirical measures of metastability after traumatic brain injury predict cognitive performance

To investigate whether empirical measures of global metastability relate to the cognitive impairments seen in the TBI population, we regressed measures of metastability against measures of cognitive flexibility, associative memory, and information processing speed, including age and mean absolute movement during the fMRI run as covariates of no interest. In patients, there was a significant negative relationship between global metastability and switch cost index (SCI, where higher SCI suggests poorer flexibility) (t_{58}=-2.21, p<0.05, Figure 6 Top) and median reaction time (t_{44}=-3.46, p<0.01, Figure 6 Middle). Global metastability was positively related to immediate memory recall, i.e. improved performance (t_{58}=2.49, p<0.05, Figure 6 Bottom), and retention (t_{58}=2.780, p<0.01, Figure 6 Bottom). These results were from a multiple regression model containing age, motion and total gray matter volume as covariates of no interest. The results survive multiple comparison correction with FDR (q<0.1).

Frontal disconnection following TBI predicts global measures of empirical metastability

We explored how regional structural disconnection may relate to metastability. We calculated the mean FA across the whole white matter skeleton and compared it with global metastability, in patients and controls, with age as a covariate of no interest. We observed a significant main effect of group (t_{84}=-2.12, $p<0.05$) and interaction between group and FA (t_{84}=2.04, $p<0.05$). We further explored this relationship at a regional level, performing a voxelwise regression of metastability on FA within both groups separately. In healthy control subjects, no region of the white matter skeleton was significantly associated with global metastability. Within the patient group, there was a significant association between global metastability and integrity of the white matter skeleton, predominantly within the white matter linking the frontal lobe with the thalamus through the anterior thalamic radiation (Figure 7). However, when the two groups were compared directly, there were no voxels surviving multiple comparison correction for a group by FA interaction, so these group differences should be treated with some caution.

A computational simulation of macroscopic neural dynamics resembles empirically-defined intrinsic connectivity networks

In order to explore how measures of metastable neural dynamics responds to structural disconnection (i.e. after TBI), we explored a computational simulation of the brain at rest using the Kuramoto model, constrained by the white matter structural connectivity between 164 brain regions, defined using white matter tractography. We validated the model by comparison with resting-state functional connectivity derived from fMRI BOLD.

Previous work has explored the dynamics of the Kuramoto model in relation to the strength and structure of coupling between nodes (Shanahan, 2010; Cabral et al., 2011; Cabral et al., 2012; Wildie and Shanahan, 2012). This work suggests that the model behaviour is highly sensitive to two constants, the global coupling parameter

(K) and mean global velocity ⟨V⟩, which is determined by a distance matrix ⟨D⟩. In order to understand the effects of these constants on our 164 node model, using coupling defined by the reference binary reference connectivity matrix (see: 'Estimation of healthy structural connectivity network'), we performed a parameter space search using 6000 randomly generated pairs of parameters $\langle k, v \rangle$, within the plane $k_{(1\ldots6)}$ and $V_{(1\ldots16)}$. The behaviour of global metastability as well as mean global synchrony of the system as a function of K is shown in (Figure 8). We observed that for increasing values of K, the system tends towards maximum global synchrony, after passing through an intermediate phase where metastability is maximal. To reduce the complexity of further computations, we selected a point in the ⟨V⟩ dimension based on plausible physiology, such that ⟨V⟩=11ms^{-1}, following (Cabral et al., 2011).

For the model output for each $\langle k, v \rangle$ pair, we used independent component analysis (ICA) to decompose the 164 node time courses into a set of simulated ICNs. These simulated ICNs were then correlated with a set of resting-state networks derived from the empirical BOLD fMRI resting state data in the same 10 independent healthy control subjects used in the tractography step (see Materials and Methods). We found that the correlation between the simulated and empirically defined networks was highest near the point of maximal metastability (Figure 8). The emergence of functional networks around the region of maximal metastability suggests that such a rich dynamical regime is an important organising principle of how structural connectivity may allow functional networks to form in the brain.

Empirically-defined macroscopic structural disconnection leads to reduced metastability in a simulation of macroscopic neural dynamics

To examine the effect of macroscopic structural disconnection following TBI on simulated neural dynamics, we used individualised structural connectivity matrices in

patients and controls (see Materials and Methods, Figure 2C) to define coupling within the Kuramoto model (Figure 1B). Global metastability was calculated for simulations of the model executed separately for each subject's connectivity matrix. Runs were repeated for a range of values of the coupling constant, K (Figure 9 Left). In the region of ideal maximum metastability identified in the parameter search (K=3.5, see above), global metastability was significantly reduced in patients compared to controls (t_{84}=-4.90, p<0.0001) (Figure 9 Right).

To further explore the effect of structural disconnection on simulated dynamics, we applied the same analysis to compute metastability within subsets of regions involved in canonical ICNs. Simulations using structural connectivity from individual TBI patients had significantly lower metastability within the dorsal attention network (t_{84}=4.15, p<0.001), a right fronto-parietal network (t_{84}=-1.99, p<0.05), default mode network (t_{84}=-3.75, p<0.001), salience network (t_{84}=-3.62, p<0.001), primary auditory (t_{84}=-4.06, p<0.001) and low-level visual networks (t_{84}=-2.45, p<0.02). Simulated results were obtained from multiple regression using age and total gray matter volume as covariates of no interest and are FDR corrected for multiple comparisons (q<0.1).

We assessed how well the simulated metastability predicts empirical metastability. Global empirical metastability was entered as the dependent variable of a linear regression, with global simulated metastability as a predictor variable, and age, total gray matter volume, and the motion estimate for the empirical data as covariates of no interest. The overall model was able to significantly predict empirical measures of metastability (F_{83} =5.95, R^2 = 0.24, P<0.0001), with a significant effect of simulated metastability (T_{83} = 3.30, P<0.001)

To evaluate the extent to which global simulated metastability is determined by changes to macroscopic structural connectivity, we used linear regression with graph

theoretical measures and group (patients or controls) as a covariate. This analysis showed small world index (t_{84}=2.91, p<0.001), clustering coefficient (t_{84}=2.36, p<0.05) and mean degree (t_{84}=5.96, p<0.001), were significant positive predictors of simulated global metastability. An increase in characteristic path length was associated with reduced metastability (t_{84}=-5.62, p<0.001).

Discussion

We considered two interrelated questions: how does high-level behaviour arise from the structural connectivity of the brain; and how does disruption of network structure alter behaviour? Metastability has been suggested as a fundamental property of neural dynamics, serving as a conceptual bridge between brain structure and behaviour (Tognoli and Kelso, 2014). Here, we used traumatic brain injury (TBI) as a model to interrogate the relationship between metastability (here defined as the standard deviation of the Kuramoto order parameter), structural connectivity and behaviour. Following TBI, metastability measured using fMRI is reduced compared to age-matched healthy control subjects. The level of metastability relates to behavioural impairment on a range of cognitive tasks. Importantly, using both empirical and computational modelling, we show that reduction in metastability following TBI is associated with damage to structural network topology, providing a demonstration of how metastable dynamics relate to behaviour through structural connectivity.

Diffuse axonal injury (DAI) is a common pathology in TBI, accounting for much of the morbidity and mortality after injury, preferentially damaging long-distance tracts (Adams et al., 1989; Geddes et al., 1997). We demonstrate a significant reduction in the ‘small-worldness’ of the structural connectome in TBI patients compared to controls, alongside a reduction in metastability. Previously, the relationship between network topology and metastability has been shown in computational simulations (Shanahan, 2010; Wildie and Shanahan, 2012); (Cabral et al., 2012). Our computational findings, alongside empirical observations, provide further support for a relationship between altered topology and metastable dynamics. We show that this relationship depends on the amount of structural damage (e.g., mean FA and average node strength) but also it depends on higher-order metrics such as

clustering coefficient and small-worldness. The relationship between small-worldness of the structural connectome and metastability makes intuitive sense. Short overall path lengths facilitate increased global synchronization, while local modular architecture may provide some reservoir of different states, preventing the system from getting "stuck" in a synchronized state. However, the relationship between network topology and metastability may not be straightforward, involving heterogeneous time delays between nodes. Alternative descriptions of the network structure may be more effective at relating damage to altered metastability (e.g., the importance of scale-free, or rich club structure (Senden et al., 2014)); more computational and theoretical work is needed.

Our modelling results support the empirical findings, demonstrating that alterations in structural topology from TBI reduce simulated metastability. This suggests a mechanistic link between reduction in small-worldness and neural dynamics. The results of the simulations are consistent with computational models based on abstract network architectures (Friston, 1997; Shanahan, 2010) and those defined by anatomical connectivity (Deco et al., 2009b; Cabral et al., 2011). This work suggests how network topology allows the emergence of metastability, implicating sparseness (Friston, 1997) and small-worldness (Shanahan, 2010; Cabral et al., 2011; Cabral et al., 2012; Wildie and Shanahan, 2012; Messe et al., 2014). More recently, networks with "rich-club" organization have been shown to support a broad repertoire of dynamic states (Senden et al., 2014). Such rich dynamics are reminiscent of the emergence of metastability; however, such a link is speculative. Future work could explore in more detail whether other graph theoretical properties, such as the presence of a strong "rich club", better explain the alterations in metastability that we observed, leading to a more refined explanation of how complex neural dynamics emerge from the network topology of the brain.

Our FMRI empirical results were acquired at rest, in the absence of any explicit behavioural requirements. The rest state is when metastability is likely to be best suited to efficient cognitive flexibility. Rest, which must be distinguished from low arousal states such as sleep or sedation, can be thought of as a “jack-of-all-trades” state when the brain is in a broad exploratory regime. The dynamical regime during at rest may constitute an upper limit for flexibility of the neural dynamics. We have previously shown, with both empirical and computational approaches, that metastability at rest is higher than during a focused cognitive task (Hellyer et al., 2014). During a task, high metastability is less desirable, since a specific configuration of brain systems is recruited (e.g., in coordinating specific visual and motor systems to perform a visually cued motor task). However, the dynamical regime during this task will still reflect the level of metastability at rest, in terms of how the system can transition from rest to a task state efficiently and reliably. With low metastability at rest (e.g. following TBI), the system is likely to take longer and be less reliable, transitioning between cognitive states, showing a reduced repertoire of brain configurations required to facilitate task performance.

Metastability may be consistent with other descriptions of the brain as a dynamical system, such as self-organised criticality. Critical systems balance the competing demands of information propagation around a system with the need to maintain stable functional long and short scale functional relationships (Beggs and Plenz, 2003; Beggs, 2008). Such behaviours maximise information flow and capacity (Shew and Plenz, 2013) which is likely important for efficient cognitive function. Previous empirical work has provided evidence of metastable dynamics in systems demonstrating signatures of self-organised criticality (Haldeman and Beggs, 2005; Kitzbichler et al., 2009). A closely related question is whether metastable dynamics underlie cognitive function at finer spatio-temporal scales, in common with other

measurements of brain activity and structure that show “scale-free” properties (Werner, 2007). Within the framework of self-organised criticality, an alteration in metastability may accompany a shift away from the critical state, associated with a decrease in efficiency of information storage, or processing capacity of the brain. Such a description has an intuitive link to cognitive deficits post TBI. The extent to which this change in metastable activity is invariant of scale (i.e. is present at the level of microscopic neural circuits as well as the macroscopic scale) is unclear. If metastability is indicative of a self-organised critical system then it may be expected that the macroscopic dynamics changes described here may cascade across all spatial and temporal scales of the brain - from local neuronal circuits to the systems level description explored here. Examination of neural dynamics at a range of spatial and temporal scales using electrophysiological or optogenetic approaches in behaving animal models (e.g. Scott et al., 2014) may therefore be helpful in exploring these mechanisms in more detail.

We found reduction in metastability related to cognitive impairments on three tasks assessed: cognitive flexibility, speed of information processing and associative memory. The switch cost index of the Trail Making Test, which involves rapidly and accurately switching between competing task demands, assesses cognitive flexibility and intuitively maps onto reduced metastability (which reflects reduced dynamical flexibility). This relationship may help explain *perseveration* following TBI: structural damage to white matter tracts limits the metastability of the brain which limits cognitive flexibility. However, the relationship between metastability and behaviour was not specific to cognitive flexibility, being present for the other two measures tested. All three tasks involve the integration of information across large-scale brain networks (Sharp et al., 2010b; Spreng and Grady, 2010; Bonnelle et al., 2011; Erika-Florence et al., 2014; Jilka et al., 2014). These tasks require communication between

sensory, motor and cognitive control regions, so altered global metastability may affect them all. This suggests large-scale metastability may be an important dynamical mechanism underlying general cognitive function. However, there may be different ways metastability can break down, evident as altered dynamics within specific brain networks, resulting in different profiles of impairments. The prominence of frontal network damage relating to metastability supports the clinically-established association between cognitive inflexibility and frontal lesions. Future work, with a larger group of patients, performing a broader range of behavioural tasks in the scanner, and imaging with higher temporal resolution would better characterize both across-subject variance in network metastability and associated patterns of behavioural impairment, beyond the domains studied here. Information about altered neural dynamics could provide a sensitive biomarker to stratify patients and be used to design individualized treatments, involving electrical stimulation, pharmacological intervention or neurofeedback (Sharp et al., 2014).

There are a number of limitations to the work. Our results show a relationship between metastability, individual cognitive performance and underlying structure in the TBI patients rather than in both the patients and controls. This may in part be because we had limited behavioural data on the healthy control subjects; also patients tend to be much more variable (in terms of behavioural impairment, neural dynamics and structure), and therefore relationships may be easier to detect. However, we also acknowledge that the lack of relationships in the healthy controls mean we can not claim that metastability is important for understanding individual differences in cognitive performance or structural network topology, beyond the patient group. A second limitation is based on the constraints inherent in tractography measured with diffusion MR. The structural connectivity matrices and graphs generated were undirected, in so much as feed-forward and feed-back connectivity of

individual regions had a uniform effect on node-node functional interaction, which is unlikely to be the case in vivo. In addition, long distance connections, for example inter-hemispheric pathways, may be difficult to resolve accurately since uncertainty in streamline location increases with the length of the tract (Jones, 2010b, a). The computational model, a system of coupled oscillators, is obviously a dramatic simplification of brain function. For example, the simulation is built on a relatively low-dimensional connectivity matrix of 164 regions. However, despite these limitations, the simulation provides important insights into the relationship between brain structure and function, broadly consistent with empirical findings. Such models, at least at the level of global network dynamics, replicate the broad changes in BOLD seen with fMRI, even though the model is based only on network topology (Deco et al., 2008; Deco et al., 2009b; Cabral et al., 2011; Cabral et al., 2012; Messe et al., 2014), with no modelling of the functional specialisation of individual nodes. These limitations mean that precise, quantitative comparisons between the simulations and the brain were not expected, although perform surprisingly well. Future work could consider whether our findings generalise to other computational oscillators models at comparable scales, such as the Wilson-Cowan model. Difficulties with the measurement of BOLD fMRI signal, such as partial volume effects, regional differences in vascular reactivity or susceptibility artefacts would also make quantitative comparisons challenging. Finally, the data we present here was collected in eyes closed state. Recent work has suggested subjects may not consistently remain conscious throughout an extended resting scan (Tagliazucchi and Laufs, 2014). This opens up the possibility that subjects varied in whether they drifted in and out of sleep and this could have affected empirical measurements of metastability. Therefore, future work, should exclude this possibility, with the use of concurrent EEG to directly detect sleep states (Tagliazucchi and Laufs, 2014).

In summary, we found large-scale structural disconnection is associated with reduced metastability, linked to impaired cognitive flexibility and other behavioural impairments. The link between damaged structural connectivity following TBI and reduced metastability (demonstrated both in empirical and simulated data) provides evidence that metastability is contingent on the integrity of the underlying structural network topology. This suggests a mechanistic link between structure, neural dynamics and behaviour. The results indicate a compelling link between brain structure and function, and suggest the framework of metastable dynamics offers an account for understanding the brain in health and disease.

References

Acebrón J, Bonilla L, Pérez Vicente C, Ritort F, Spigler R (2005) The Kuramoto model: A simple paradigm for synchronization phenomena. Reviews of Modern Physics 77:137-185.

Adams JH, Doyle D, Ford I, Gennarelli TA, Graham DI, McLellan DR (1989) Diffuse axonal injury in head injury: definition, diagnosis and grading. Histopathology 15:49-59.

Baddeley A (1986) Working Memory. Oxford: Clarendon Press.

Baddeley A (1992) Working memory. Science 255:556-559.

Baddeley AD, Emslie H, Nimmo-Smith I (1994) Doors and people: A test of visual and verbal recall and recognition: Thames Valley Test Company.

Bassett DS, Bullmore E (2006) Small-world brain networks. The Neuroscientist : a review journal bringing neurobiology, neurology and psychiatry 12:512-523.

Beckmann CF, DeLuca M, Devlin JT, Smith SM (2005) Investigations into resting-state connectivity using independent component analysis. Philos Trans R Soc Lond B Biol Sci 360:1001-1013.

Behrens TE, Johansen-Berg H, Woolrich MW, Smith SM, Wheeler-Kingshott CA, Boulby PA, Barker GJ, Sillery EL, Sheehan K, Ciccarelli O, Thompson AJ, Brady JM, Matthews PM (2003a) Non-invasive mapping of connections between human thalamus and cortex using diffusion imaging. Nat Neurosci 6:750-757.

Behrens TEJ, Woolrich MW, Jenkinson M, Johansen-Berg H, Nunes RG, Clare S, Matthews PM, Brady JM, Smith SM (2003b) Characterization

and propagation of uncertainty in diffusion-weighted MR imaging. Magnetic Resonance in Medicine 50:1077-1088.

Bhowmik D, Shanahan M (2013) Metastability and inter-band frequency modulation in networks of oscillating spiking neuron populations. PloS one 8:e62234.

Bird CM, Castelli F, Malik O, Frith U, Husain M (2004) The impact of extensive medial frontal lobe damage on 'Theory of Mind' and cognition. Brain 127:914-928.

Bonnelle V, Ham TE, Leech R, Kinnunen KM, Mehta MA, Greenwood RJ, Sharp DJ (2012) Salience network integrity predicts default mode network function after traumatic brain injury. Proceedings of the National Academy of Sciences of the United States of America 109:4690-4695.

Bonnelle V, Leech R, Kinnunen KM, Ham TE, Beckmann CF, De Boissezon X, Greenwood RJ, Sharp DJ (2011) Default Mode Network Connectivity Predicts Sustained Attention Deficits after Traumatic Brain Injury. J Neurosci 31:13442-13451.

Cabral J, Hughes E, Sporns O, Deca G (2011) Role of local network oscillations in resting-state functional connectivity. NeuroImage 57:130 - 139.

Cabral J, Hugues E, Kringelbach ML, Deco G (2012) Modeling the outcome of structural disconnection on resting-state functional connectivity. NeuroImage 62:1342-1353.

Caeyenberghs K, Leemans A, Leunissen I, Gooijers J, Michiels K, Sunaert S, Swinnen SP (2014) Altered structural networks and executive deficits in traumatic brain injury patients. Brain structure & function 219:193-209.

Chang C, Glover GH (2010) Time,Äìfrequency dynamics of resting-state brain connectivity measured with fMRI. NeuroImage 50:81-98.

Chialvo DR (2010) Emergent complex neural dynamics. Nature Physics 6:744-750.

Deco G, Rolls ET, Romo R (2009a) Stochastic dynamics as a principle of brain function. Progress in Neurobiology 88:1--16.

Deco G, Jirsa VK, Robinson PA, Breakspear M, Friston K (2008) The Dynamic Brain: From Spiking Neurons to Neural Masses and Cortical Fields. PLoS Comput Biol 4:e1000092.

Deco G, Jirsa V, McIntosh AR, Sporns O, Kotter R (2009b) Key role of coupling, delay, and noise in resting brain fluctuations. Proc Natl Acad Sci U S A 106:10302-10307.

Erika-Florence M, Leech R, Hampshire A (2014) A functional network perspective on response inhibition and attentional control. Nature communications 5:4073.

Fischl B, van der Kouwe A, Destrieux C, Halgren E, Segonne F, Salat DH, Busa E, Seidman LJ, Goldstein J, Kennedy D, Caviness V, Makris N, Rosen B, Dale AM (2004) Automatically parcellating the human cerebral cortex. Cerebral cortex 14:11-22.

Freeman LC (1978) Segregation in Social Networks. Sociol Method Res 6:411-429.

Friston KJ (1997) Transients, metastability, and neuronal dynamics. NeuroImage 5:164-171.

Friston KJ (2002) Dysfunctional connectivity in schizophrenia. World psychiatry : official journal of the World Psychiatric Association (WPA) 1:66-71.

Friston KJ, Mechelli A, Turner R, Price CJ (2000) Nonlinear responses in fMRI: the Balloon model, Volterra kernels, and other hemodynamics. Neuroimage 12:466-477.

Geddes JF, Vowles GH, Beer TW, Ellison DW (1997) The diagnosis of diffuse axonal injury: implications for forensic practice. Neuropathol Appl Neurobiol 23:339-347.

Gigandet X, Hagmann P, Kurant M, Cammoun L, Meuli R, Thiran JP (2008) Estimating the confidence level of white matter connections obtained with MRI tractography. PLoS One 3:e4006.

Glerean E, Salmi J, Lahnakoski JM, Jaaskelainen IP, Sams M (2012) Functional magnetic resonance imaging phase synchronization as a measure of dynamic functional connectivity. Brain connectivity 2:91-101.

Gong G, He Y, Concha L, Lebel C, Gross DW, Evans AC, Beaulieu C (2009) Mapping anatomical connectivity patterns of human cerebral cortex using in vivo diffusion tensor imaging tractography. Cerebral cortex 19:524-536.

Gratton C, Nomura EM, Perez F, D'Esposito M (2012) Focal brain lesions to critical locations cause widespread disruption of the modular

organization of the brain. Journal of cognitive neuroscience 24:1275-1285.

Greve DN, Fischl B (2009) Accurate and robust brain image alignment using boundary-based registration. NeuroImage 48:63--72.

Hagmann P, Cammoun L, Gigandet X, Meuli R, Honey CJ, Wedeen VJ, Sporns O (2008) Mapping the structural core of human cerebral cortex. PLoS biology 6:e159.

Haldeman C, Beggs JM (2005) Critical branching captures activity in living neural networks and maximizes the number of metastable States. Phys Rev Lett 94:058101.

Hellyer PJ, Leech R, Ham TE, Bonnelle V, Sharp DJ (2013) Individual prediction of white matter injury following traumatic brain injury. Annals of Neurology 73:489-499.

Hellyer PJ, Shanahan M, Scott G, Wise RJ, Sharp DJ, Leech R (2014) The control of global brain dynamics: opposing actions of frontoparietal control and default mode networks on attention. The Journal of Neuroscience 34:451-461.

Honey CJ, Sporns O, Cammoun L, Gigandet X, Thiran JP, Meuli R, Hagmann P (2009) Predicting human resting-state functional connectivity from structural connectivity. Proc Natl Acad Sci U S A 106:2035-2040.

Humphries MD, Gurney K (2008) Network 'Small-World-Ness': A Quantitative Method for Determining Canonical Network Equivalence. Plos One 3.

Jilka S, Scott G, Ham TE, Pickering A, Bonnelle V, Braga R, Leech R, Sharp DJ (2014) Damage to the Salience Network and Interactions with the Default Mode Network. The Journal of Neuroscience 34:10798-10807.

Johnson VE, Stewart W, Smith DH (2013a) Axonal pathology in traumatic brain injury. Experimental neurology 246:35-43.

Johnson VE, Stewart JE, Begbie FD, Trojanowski JQ, Smith DH, Stewart W (2013b) Inflammation and white matter degeneration persist for years after a single traumatic brain injury. Brain : a journal of neurology 136:28-42.

Jones DK (2010a) Precision and Accuracy in Diffusion Tensor Magnetic Resonance Imaging. Topics in Magnetic Resonance Imaging 21:87-99.

Jones DK (2010b) Challenges and limitations of quantifying brain connectivity in vivo with diffusion MRI. Imaging in Medicine 2:341-355.

Kinnunen KM, Greenwood R, Powell JH, Leech R, Hawkins PC, Bonnelle V, Patel MC, Counsell SJ, Sharp DJ (2011) White matter damage and cognitive impairment after traumatic brain injury. Brain 134:449-463.

Kitzbichler MG, Smith ML, Christensen SoR, Bullmore E (2009) Broadband criticality of human brain network synchronization. PLoS Computational Biology 5:e1000314.

Kuramoto Y (1984) Chemical oscillations, waves, and turbulence. New York: Springer.

Logan GD, Cowan WB, Davis KA (1984) On the ability to inhibit simple and choice reaction time responses: a model and a method. Journal of experimental psychology 10:276-291.

Malec JF, Brown AW, Leibson CL, Flaada JT, Mandrekar JN, Diehl NN, Perkins PK (2007) The mayo classification system for traumatic brain injury severity. J Neurotrauma 24:1417-1424.

Messe A, Rudrauf D, Benali H, Marrelec G (2014) Relating structure and function in the human brain: relative contributions of anatomy, stationary dynamics, and non-stationarities. PLoS Comput Biol 10:e1003530.

Niazy RK, Xie J, Miller K, Beckmann CF, Smith SM (2011) Spectral characteristics of resting state networks. Progress in brain research 193:259-276.

Nichols TE, Holmes AP (2002) Nonparametric permutation tests for functional neuroimaging: a primer with examples. Human brain mapping 15:1-25.

Rabbitt P (1966) Errors and error correction in choice reaction tasks. J Exp Psychol 71:264-272.

Reitan R (1958) The validity of the Trail Making test as an indicator of organic brain damage. Perceptual and Motor Skills 8:271-276.

Rubinov M, Sporns O (2010) Complex network measures of brain connectivity: uses and interpretations. Neuroimage 52:1059-1069.

Scott G, Fagerholm ED, Mutoh H, Leech R, Sharp DJ, Shew WL, Knopfel T (2014) Voltage imaging of waking mouse cortex reveals emergence of critical neuronal dynamics. The Journal of neuroscience : the official journal of the Society for Neuroscience 34:16611-16620.

Senden M, Deco G, de Reus MA, Goebel R, van den Heuvel MP (2014) Rich club organization supports a diverse set of functional network configurations. Neuroimage 96:174-182.

Shanahan M (2010) Metastable chimera states in community-structured oscillator networks. Chaos: An Interdisciplinary Journal of Nonlinear Science 20:013108}.

Sharp DJ, Scott G, Leech R (2014) Network dysfunction after traumatic brain injury. Nature reviews Neurology 10:156-166.

Sharp DJ, Turkheimer FE, Bose SK, Scott SK, Wise RJ (2010a) Increased frontoparietal integration after stroke and cognitive recovery. Ann Neurol 68:753-756.

Sharp DJ, Bonnelle V, De Boissezon X, Beckmann CF, James SG, Patel MC, Mehta MA (2010b) Distinct frontal systems for response inhibition, attentional capture, and error processing. Proceedings of the National Academy of Sciences of the United States of America 107:6106-6111.

Sharp DJ, Beckmann CF, Greenwood R, Kinnunen KM, Bonnelle V, De Boissezon X, Powell JH, Counsell SJ, Patel MC, Leech R (2011) Default mode network functional and structural connectivity after traumatic brain injury. Brain : a journal of neurology 134:2233-2247.

Shew WL, Plenz D (2013) The functional benefits of criticality in the cortex. The Neuroscientist : a review journal bringing neurobiology, neurology and psychiatry 19:88-100.

Smith SM, Jenkinson M, Johansen-Berg H, Rueckert D, Nichols TE, Mackay CE, Watkins KE, Ciccarelli O, Cader MZ, Matthews PM, Behrens TE

(2006) Tract-based spatial statistics: voxelwise analysis of multi-subject diffusion data. Neuroimage 31:1487-1505.

Smith SM, Fox PT, Miller KL, Glahn DC, Fox PT, Mackay CE, Filippini N, Watkins KE, Toro R, Laird AR, Beckmann CF (2009) Correspondence of the brain's functional architecture during activation and rest. Proceedings of the National Academy of Sciences of the United States of America 106:13040--13045.

Smith SM, Jenkinson M, Woolrich MW, Beckmann CF, Behrens TE, Johansen-Berg H, Bannister PR, De Luca M, Drobnjak I, Flitney DE, Niazy RK, Saunders J, Vickers J, Zhang Y, De Stefano N, Brady JM, Matthews PM (2004) Advances in functional and structural MR image analysis and implementation as FSL. Neuroimage 23 Suppl 1:S208-219.

Sporns O (2006) Small-world connectivity, motif composition, and complexity of fractal neuronal connections. Biosystems 85:55-64.

Spreng RN, Grady CL (2010) Patterns of brain activity supporting autobiographical memory, prospection, and theory of mind, and their relationship to the default mode network. Journal of cognitive neuroscience 22:1112-1123.

Squarcina L, Bertoldo A, Ham TE, Heckemann R, Sharp DJ (2012) A robust method for investigating thalamic white matter tracts after traumatic brain injury. Neuroimage 63:779-788.

Strogatz SH (2001) Exploring complex networks. Nature 410:268-276.

Tagliazucchi E, Laufs H (2014) Decoding wakefulness levels from typical fMRI resting-state data reveals reliable drifts between wakefulness and sleep. Neuron 82:695-708.

Tognoli E, Kelso JAS (2014) The Metastable Brain. Neuron 81:35-48.

Uhlhaas PJ, Singer W (2006) Neural synchrony in brain disorders: relevance for cognitive dysfunctions and pathophysiology. Neuron 52:155-168.

van den Heuvel MP, Sporns O (2011) Rich-club organization of the human connectome. J Neurosci 31:15775-15786.

Warren DE, Power JD, Bruss J, Denburg NL, Waldron EJ, Sun H, Petersen SE, Tranel D (2014) Network measures predict neuropsychological outcome after brain injury. Proc Natl Acad Sci U S A 111:14247-14252.

Watts DJ, Strogatz SH (1998) Collective dynamics of 'small-world' networks. Nature 393:440-442.

Werner G (2007) Metastability, criticality and phase transitions in brain and its models. Bio Systems 90:496--508.

Wildie M, Shanahan M (2012) Metastability and chimera states in modular delay and pulse-coupled oscillator networks. Chaos: An Interdisciplinary Journal of Nonlinear Science 22:043131.

Winkler AM, Ridgway GR, Webster MA, Smith SM, Nichols TE (2014) Permutation inference for the general linear model. Neuroimage 92:381-397.

Legends

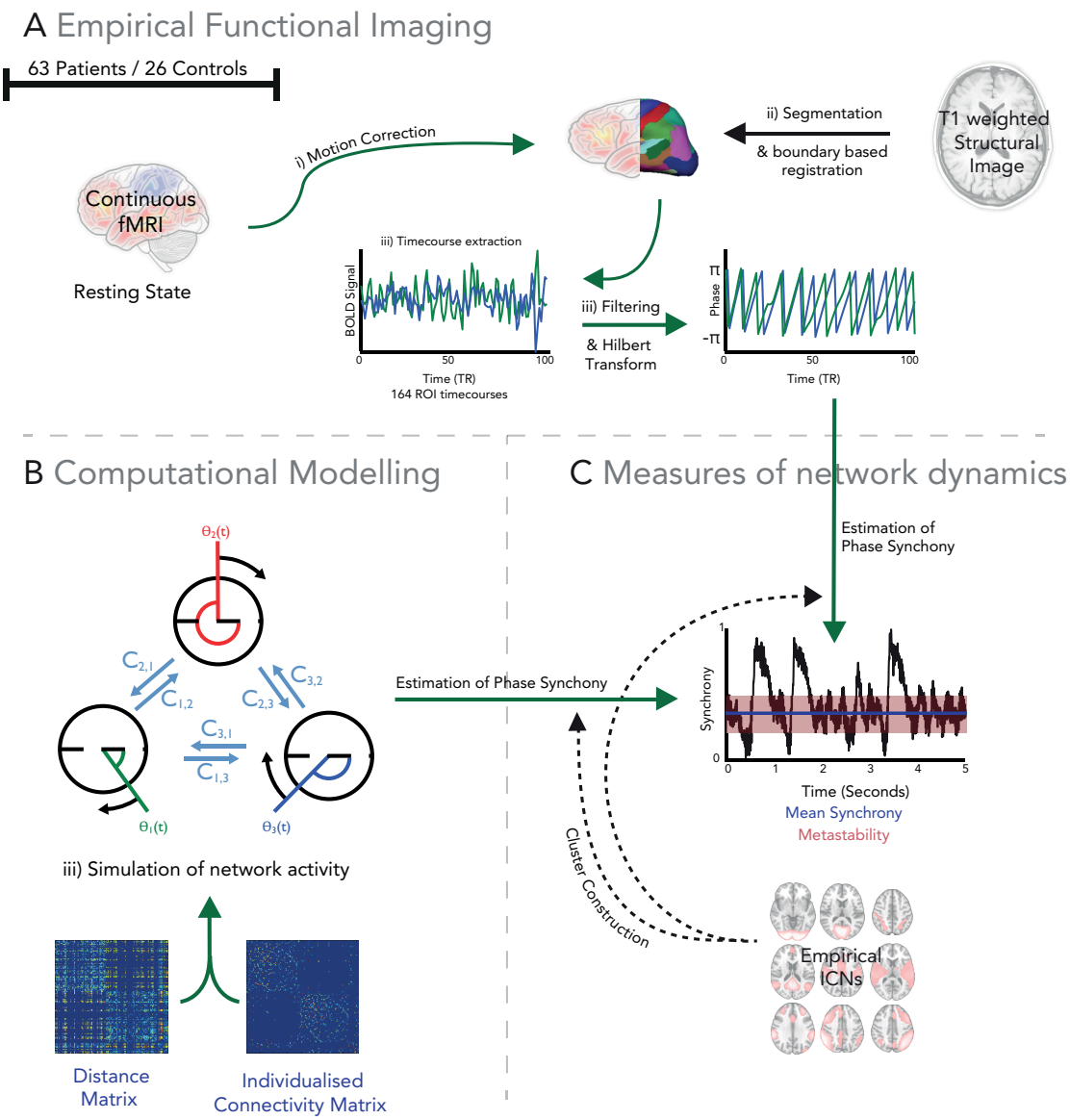

Figure 1: Overview of experimental design. ***A***, fMRI was used to estimate global measures of network dynamics during rest in 63 Patients and 26 Controls. ***B***, We used a computational model to simulate neural dynamics using dynamic systems framework constrained by structural connectivity. ***C*** We used a Hilbert transformation of the fMRI data and the phase output of the computational model to compare the global dynamics of empirical data and the dynamics of a computational model constrained by white matter structural connectivity.

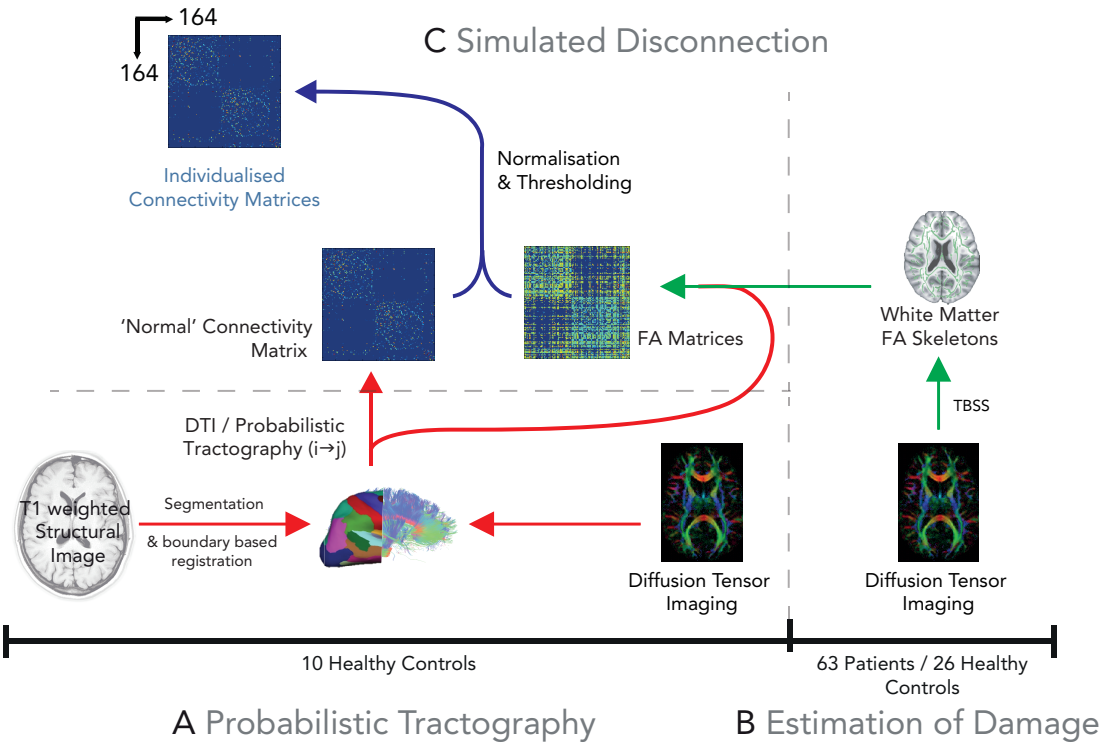

Figure 2: Estimation of structural disconnection in traumatic brain injury patients versus controls. ***A,*** To define a standardised connectivity matrix to perform computational simulation, probabilistic tractography was performed in 10 independent age matched healthy control subjects, resulting in a binary connectivity graph and spatial estimates of probable tract location for each connected edge (see materials and methods). ***B***, Measures of tract integrity (FA) were estimated in each of the 63 Patients and 26 healthy controls by generating a 'skeleton' for each subject using the pre-processing steps of TBSS. ***C***, For each edge of the reference connectivity matrix, each subject's FA skeleton was projected though the spatial mask for each edge, resulting in a 164 region 'white matter integrity' matrix for each subject. ***C***, For each subject, the reference binary connectivity map was weighted according to relative reduction in tract integrity in each individual subject (see materials and methods), resulting in a individual weighted connectivity matrix for each of the 63 TBI patients and 26 Healthy controls.

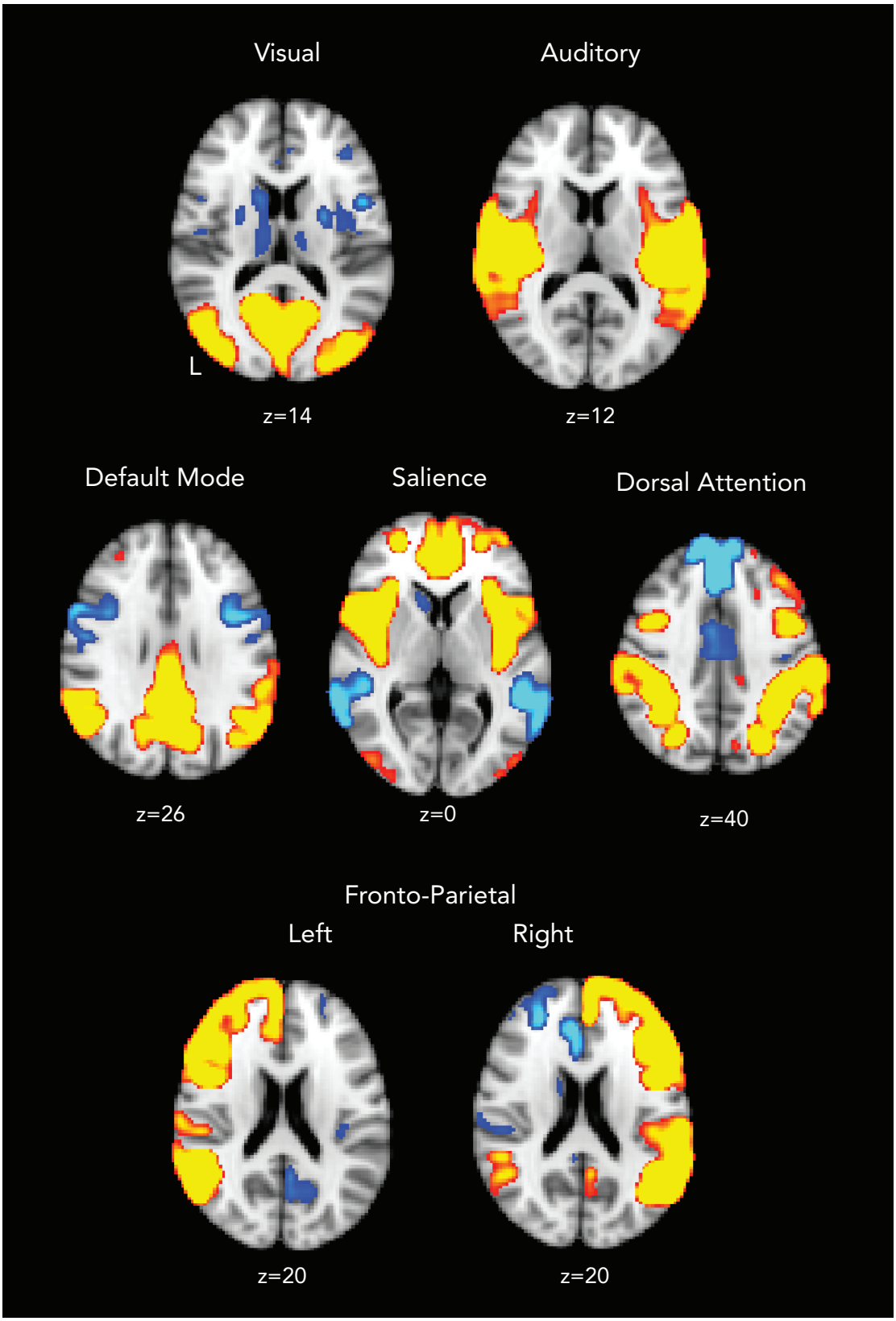

Figure 3: Independent component analysis (ICA) of fMRI data in macroscopic ROIs. ICA was used to decompose ROI data from 164 cortical and subcortical regions of the brain in 10 healthy control subjects into 15 components. Here, 7 of the

resulting components which best resembled canonical 'resting state networks' have been reconstructed into Montréal Neurological Institute (MNI) 152 space according to the 164 region model with a Gaussian blur of 3mm (isotropic) for ease of visualisation.

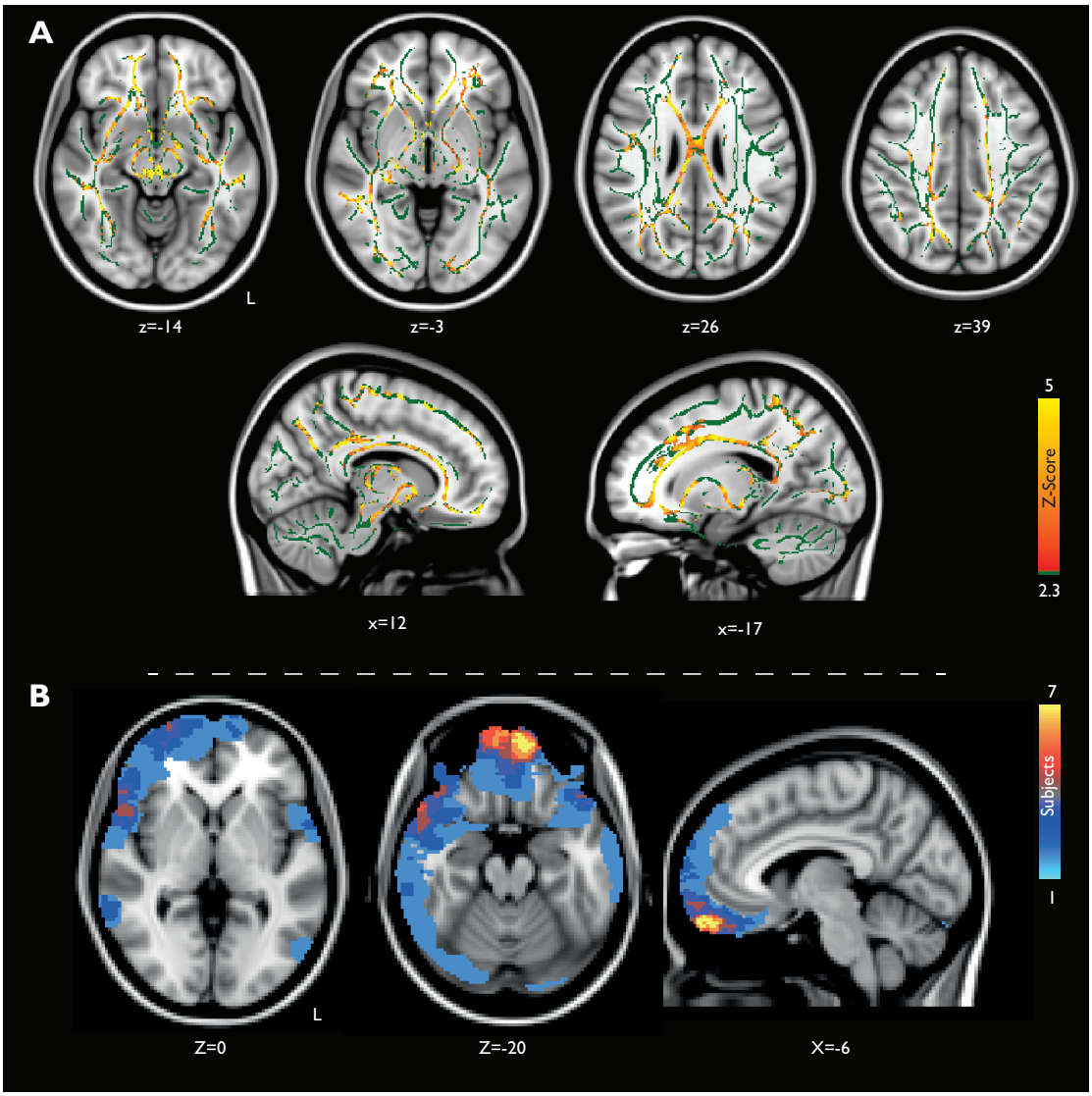

Figure 4: Structural brain damage following traumatic brain injury. *A) Widespread white matter disruption following traumatic brain injury measured by TBSS of Fractional anisotropy (FA).* Contrasts between traumatic brain injury < healthy control subjects (Red-Yellow). Contrasts overlaid on a standard Montréal Neurological Institute 152 T_1 1 mm brain and the mean FA skeleton (in green), thresholded at $P \leq 0.05$, corrected for multiple comparisons using Threshold Free

Cluster Enhancement (TFCE) (Smith et al., 2006). *B) Lesion probability maps of cortical contusions across 63 TBI patients.* Estimated by a neuroradiologist on the T1 structural images. The colour bar indicates the number of patients who had lesions at each site, overlaid on a standard Montréal Neurological Institute 152 T_1 2 mm brain.

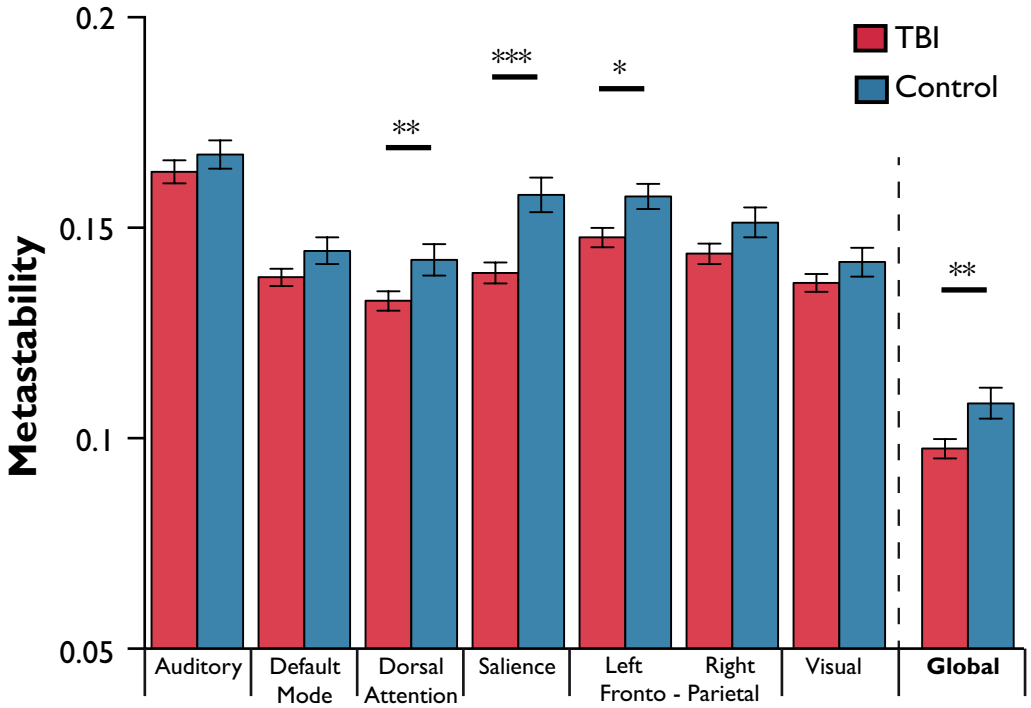

Figure 5: Empirical Metastability at rest is significantly reduced in patients compared to controls. Mean measures of metastability (±1SEM) estimated using phase transformed functional time-course extracted from 63 Patients and 26 Control subjects suggest that global measures of metastability are reduced following TBI.

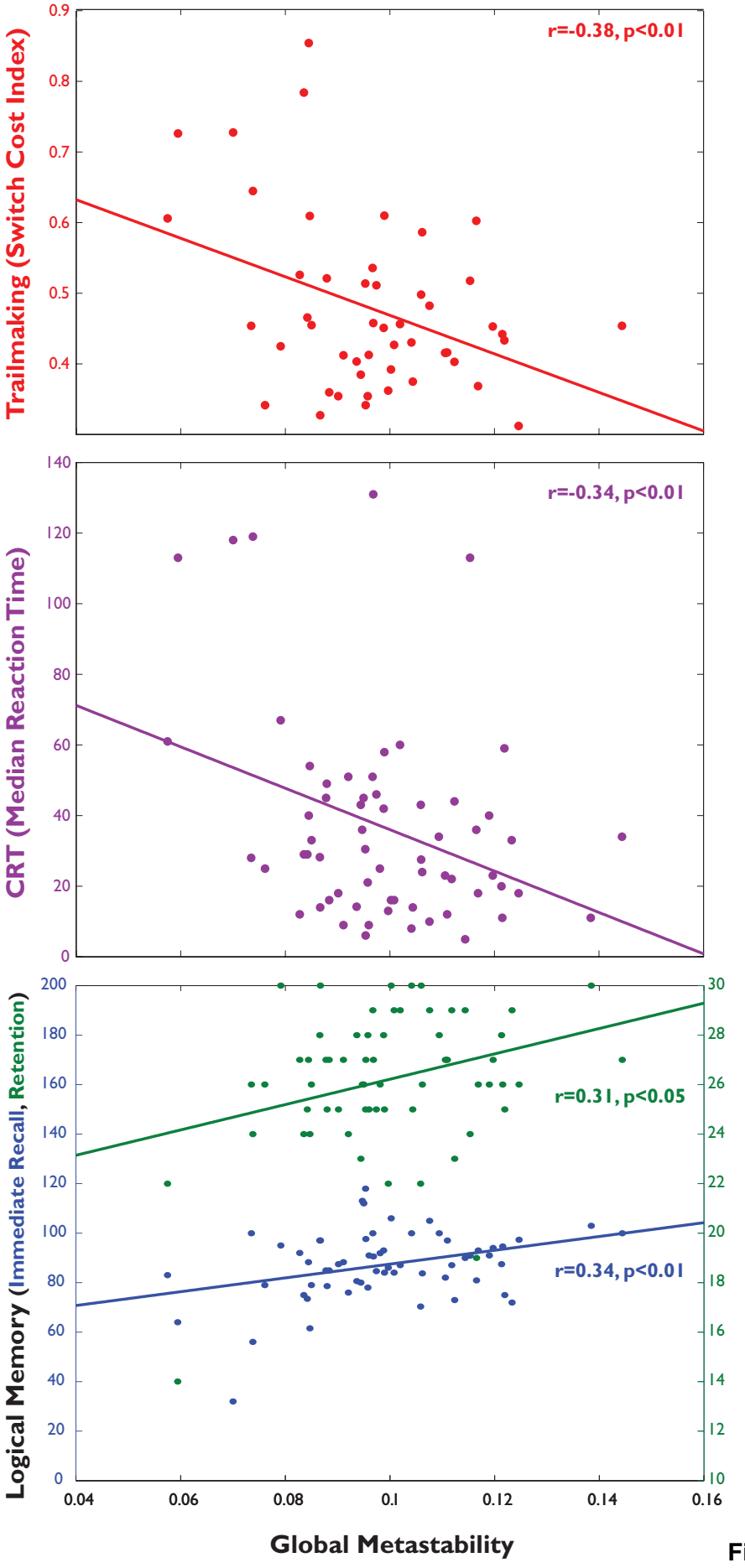

Figure 6: Global

Metastability predicts behavioural outcome. Measures of global metastability during rest significantly correlate with scores of task-switching (Top, Red n=62), Information Processing speed (Middle, Purple, n=49), and Logical Memory (Bottom, Blue and Green, n=62).

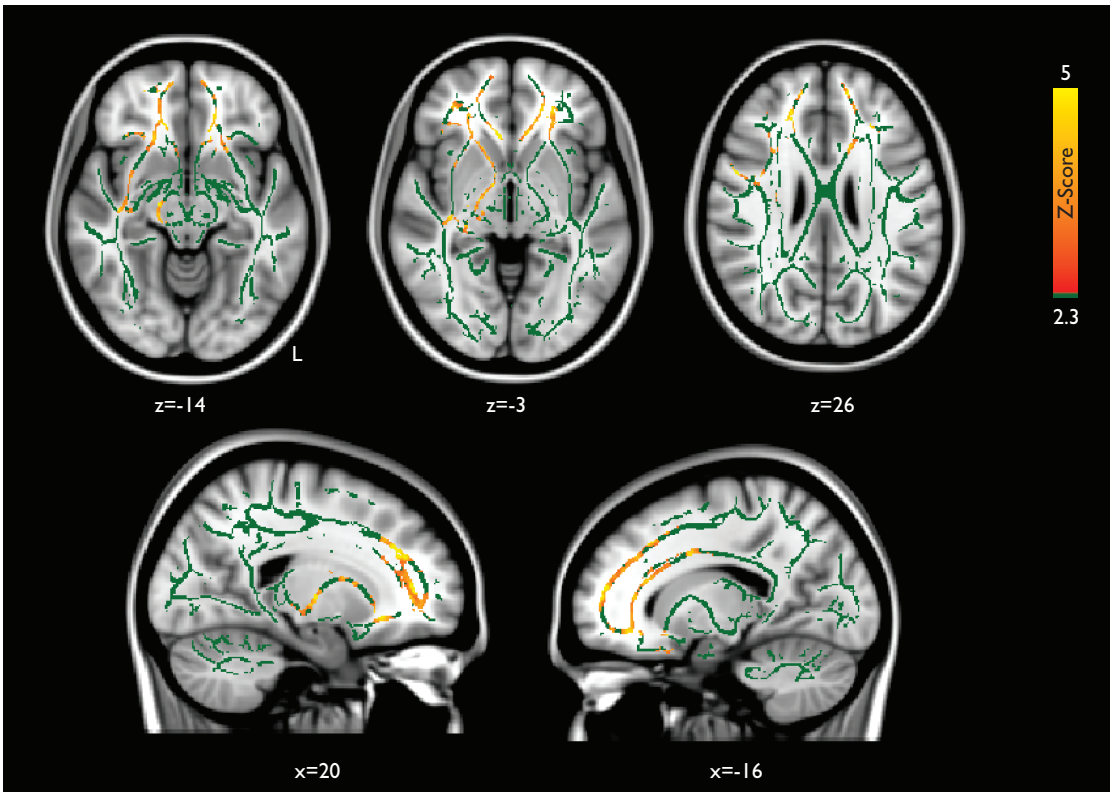

Figure 7: Empirical metastability in patients is associated with cortical connectivity within the frontal lobes. Multiple regression of empirical global metastability (Red-Yellow) with skeletonised FA values in 63 TBI patients (age included as a covariate of no interested). Results overlaid on a standard Montréal Neurological Institute 152 T_1 1 mm brain and the mean fractional anisotropy skeleton (in green), thresholded at $P \leq 0.05$, corrected for multiple comparisons using Threshold Free Cluster Enhancement (TFCE) (Smith et al., 2006).

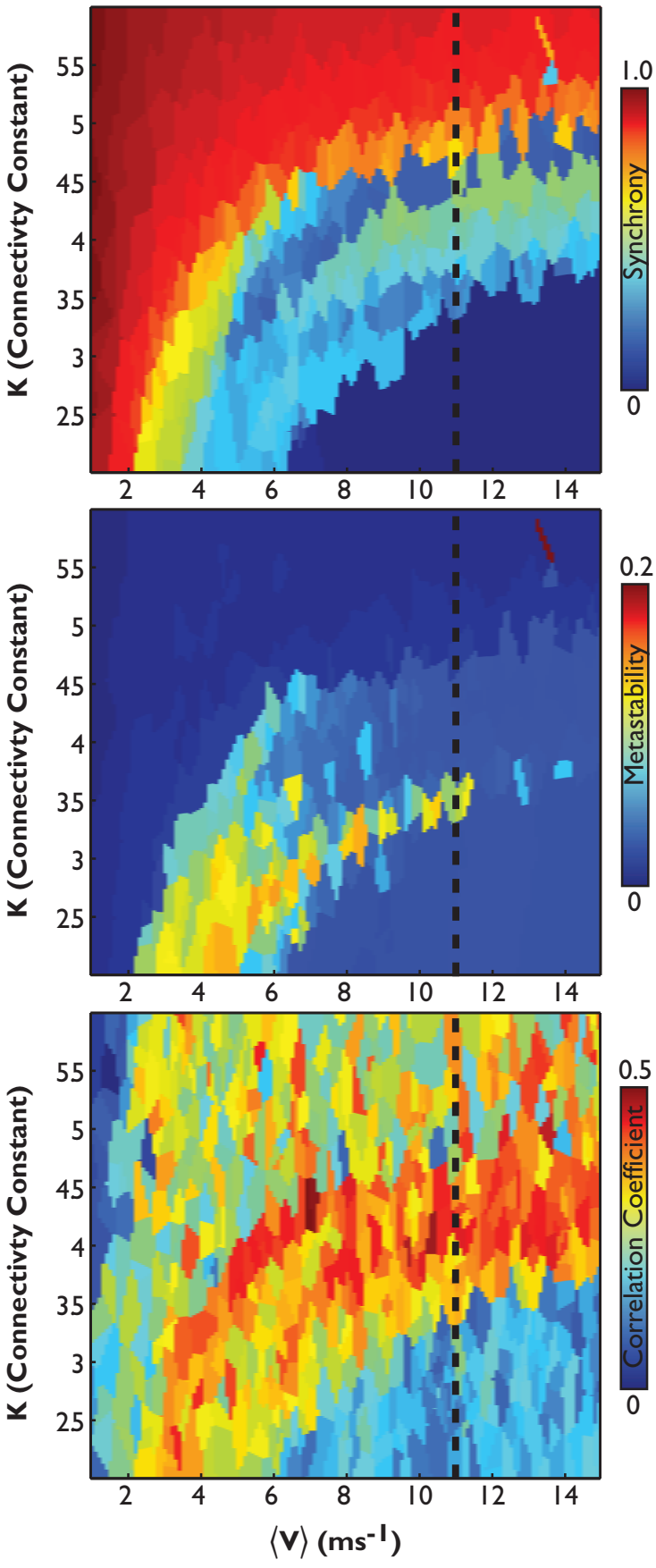
K (Connectivty Constant)
55
5
45
4
35
3
25
2
4
6
8
10
12
14
1.0
Synchrony
0
0.2
Metastability
0
0.5
Correlation Coefficient
0
⟨v⟩ (ms-1)

Figure

8: A large-scale neural network model predicts functional connectivity where metastability is maximised. Plots of a parameter space exploration of the Kuramoto model the using 6000 randomly generated pairs of the coupling and delay parameters $\langle k, v \rangle$, within the plane $k_{(1\ldots6)}$ and $V_{(1\ldots16)}$, here expressed as mean velocity (ms-1). Global Synchrony (Top). Global Metastability (Middle), and Correlations of the 5 best-matching simulated and empirical ICNs (Bottom). For ease of further computation we set velocity at a biologically plausible value (Cabral et al., 2011), which equates to ~ 11ms-1 (dashed line)

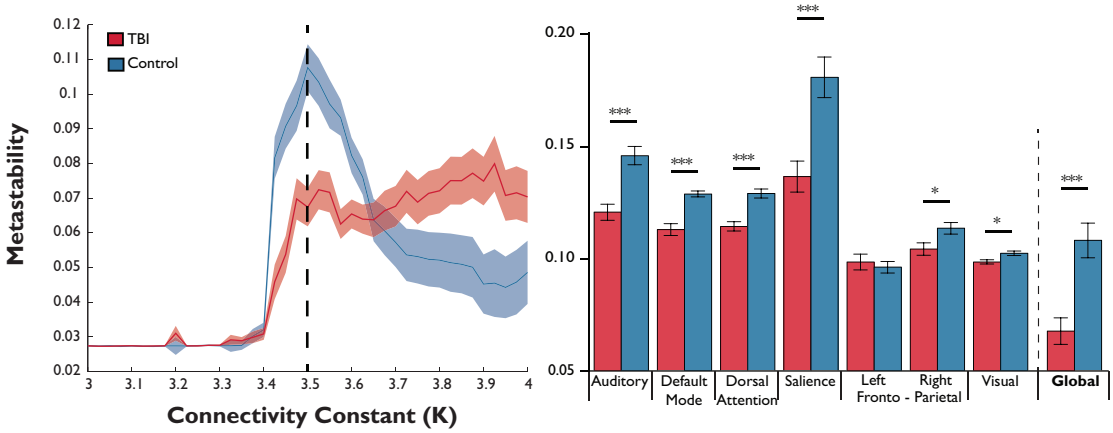

Figure 9: Simulated global metastability is decreased in traumatic brain injury patients compared to controls ***A***, Mean metastability (±1SEM) for in patients (n=63) and controls (n=26) in the computational model for a range of different coupling strengths (K). v = 11ms -1. ***B***, Mean measures of metastability estimated within the model (±1SEM) for 63 patients and 26 healthy control subjects suggest that global measures of metastability simulated from structural connectivity in TBI patients are reduced compared to healthy controls.